ingegneria sismica
International Journal of Earthquake Engineering
Anno XLIII - Num. 1 - 2026

Research on Integrated Collaborative Planning of Source, Grid, Load and Storage for Electricity Spot Markets

Zijiao Han[1], *Miao Wang*[1], *Jingwei Hu*[1], *Mingshun Ji*[2,*], *Gongyu Wei*[2] *and Qiang Yang*[2]

[1] Department of Development, State Grid Liaoning Electric Power Co., Ltd., Shenyang, Liaoning, 110006, China
[2] Beijing Tsintergy Technology Co., Ltd., Beijing, 100080, China

SUMMARY: *Based on the spot market trading mechanism of source network and load storage revenue allocation, a planning model of the joint optical storage system is constructed, which realizes the effective planning for both internal and external layers of the system under multiple constraints. The enhanced multi-objective particle swarm optimization algorithm involves a dispersal mechanism and conducts a global search of the best configuration of the integrated source-grid-load-storage system by adjusting the positions of particles, enhancing their diversity, and other similar operations. A series of experiments is conducted to test the effectiveness of such coordinated planning strategy in the context of the integrated source-grid-load-storage structure. The IMOPSO algorithm presented in this work can be well applied to models of different dimensionality and computational complexity. The findings on three planned scenarios show that in the framework of coordinated source-grid-load-storage planning, the optimal scheduling scheme and the energy cost at the operational level impact the value of the objective function and the configuration of the power generation machinery at the planning level, whereas the optimized planning-level configuration further influences the combination of unit outputs in operation. They are interrelated.*

KEYWORDS: *IMOPSO algorithm; source-grid-load-storage integration; multi-objective optimization; electricity spot market*

1 Introduction

Vigorously developing renewable energy is one of the main measures to realize China's “dual-carbon” strategic goal [1]. As the proportion of wind power, photovoltaic and other renewable energies connected to the grid expands year by year, the power grid needs more flexible resources for regulation [2, 3]. An efficient way to promote the initiative and flexibility of the new energy units along with other regulating resources is to maximize the utilization of the electricity spot market to allocate power resources. As of now, the electricity spot market of China has not yet developed into a well-developed stage whereby the trading mechanism, as well as the entire market system of the power resources, are inadequate in terms of maturity [4]. In this current reform process that seeks to further develop the power-market, studies regarding the coordination and integrated planning of source-grid-load-storage systems are thus important to the progress and construction of clean-energy system and electricity spot market of China.

The principal participants in electricity spot-market clearing mainly include energy suppliers, grid operators, energy storage providers, and load aggregators on the demand side.

*jims@tsintergy.com
https://doi.org/10.65102/is2026452
Published: 30 April, 2026

To effectively coordinate the interests of all parties and maintain stable system operation, energy suppliers, storage providers, and load aggregators may sign mutual-insurance contracts with the grid operator during the day-ahead stage [5, 6]. In day-ahead clearing, while maintaining the balance between supply and demand, integrated coordination among source, grid, load, and storage must also be achieved [7]. On the demand side, because regulation capability is relatively weak, load aggregators actively submit adjustable power bids and participate in day-ahead competition; they also enter into mutual-insurance agreements with grid operators on behalf of users, thereby reducing electricity costs [8, 9]. In addition, to support priority access for renewable generation, conventional coal-fired units, wind turbines, and photovoltaic plants may all take part in day-ahead subscriptions while simultaneously forming mutual-insurance contracts with operators [10]. Owing to the volatility of renewable energy, fluctuations are mainly smoothed by storage resources, and thus energy storage providers and grid operators establish mutual-insurance arrangements for electricity-storage services and discharge standby capacity, forming reserve regulation capability [11, 12]. finally, by creating a competitive electricity spot market environment, we get the bidding relationship between energy supply, storage and energy use, and the grid operator decides the final pricing to avoid unilateral transition monopoly phenomenon [13, 14]. The integrated collaborative planning is mainly through the grid operator for power selection and guarantee, the energy supplier, energy storage provider and load aggregator for tariff guarantee, and the reasonable distribution of the benefits of multiple parties to get the day-ahead clearing program [15-17].

This paper constructs a planning model of combined photovoltaic and storage system based on source-network-load cooperative optimization, which is divided into two aspects: outer layer planning and inner layer planning. The rational planning of the outer layer will achieve the maximization of the PV in-situ consumption rate and the investment return of the combined optical storage system, while the inner layer planning focuses on the minimization of the average value of the voltage deviation, the outer layer passes the configuration scheme of the combined optical storage system to the inner layer, and the inner layer passes the optimized implementation scheme of the active management of each scenario to the outer layer. The proposed solution to this planning problem is a more efficient multi-objective particle swarm optimization algorithm. To further ensure the validity of the enhanced approach and its efficiency in the source-grid-load-storage planning, arithmetic simulation experiments are conducted.

2 IMOPSO-based integrated collaborative planning model of source network, load and storage

2.1 Spot Market Trading Mechanisms for the Distribution of Proceeds from Source Grid Load Storage

2.1.1 Transaction mechanism for harmonization of source-network load and storage revenues

The main actors in the electricity spot-market clearing process are energy suppliers, grid operators, energy storage providers, and demand-side load aggregators. Of these, the energy suppliers are mostly conventional gas-fired units, wind turbines, and photovoltaic generation facilities that offer bids to the electricity market. Grid-based operating companies are mainly grid operators which aim at purchasing and selling power so as to ensure stable system performance. Energy storage providers are typically enterprises which meet requirements of

electricity charging and discharging at various peak and valley intervals of the grid, smooth out fluctuations due to intermittent renewable generation, and utilize their flexible multi-period storage and releasing functionality to enter into market bidding. The load aggregators can represent the interests of the demand side and may engage in day-ahead trading of selected flexible loads, which can be displaced to help with demand response. To ensure that all participants have their interests aligned whilst maintaining a stable system operation, energy suppliers, storage providers, and load aggregators will enter into electricity mutual-insurance agreements with grid operators at the day-ahead market stage. As part of that clearance procedure, it is also important to note that the income sharing between the four elements, i.e., the source, grid, load and storage should be distributed fairly. The particular transaction mechanism that would facilitate coordinated revenue sharing among the source, grid, load and storage is depicted in the Figure 1.

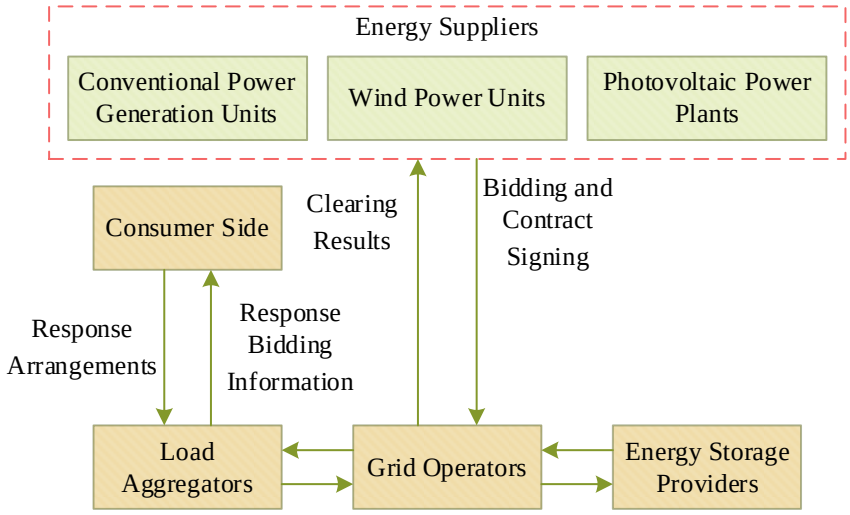

Figure 1: The trading mechanism of source-grid-load-storage

2.1.2 Price Compensation Models for Multi-Party Cost Harmonization

In spot-market clearing, the system operator should not aim at maximizing revenues only in case of different generation and flexibility resources, but consider grid safety, operational reliability, and overall system stability as well when settling the markets. Considering the diverse range of generation, demand, storage, network assets, and associated participants, one may use a multidimensional data-cube approach to find out the compensation of the different entities in the electricity market. The calculation is based on transaction records, information about the condition of equipment, customer repair requests, the log of complaints, and other massive sources of data; thus, there is some support to the more inclusive and data-oriented compensation system.According to the power grid operator's clearing power in different time periods, its compensation revenue R_{PG} is:

$$R_{PG} = \sum_{t=1}^{T} \left(Q_{PGD,t} - Q_{PGC,t} \right) C_{PGCP,t} \tag{1}$$

where $Q_{PGD,t}$, $Q_{PGC,t}$, $C_{PGCP,t}$ are the market clearing power, contracted power, and unit compensation price at time t, respectively; and T is the total number of time slots.

According to the multi-dimensional data cube model and the arithmetic database model, the

summation and aggregation model of contracted electricity is defined as:

$$Q_{PGC} = \theta_a \left(\sum (M_v), \{ d_{sp}, d_{ti} \} \right) \tag{2}$$

where Q_{PGC} is the total amount of contracted tariffs in the arithmetic database; $\theta_a(\cdot)$ is the aggregation function; M_v is the attribute of the power measure in the contract disaggregation database, i.e., the data of transacted electricity disaggregated by time slots after each trading entity has signed a contract in the process of spot trading; d_{sp}, d_{ti} are the spatial and temporal dimensions of electricity resources in the spot market, respectively. Therefore, the product expansion model of the compensation price in the database is obtained as:

Where Q_{PGC} is the total amount of contracted electricity price in the arithmetic database; $\theta_a(\cdot)$ is the aggregation function; M_v is the electricity measure attribute in the contract decomposition database, i.e., the electricity data of the transaction in the spot trading process, which is decomposed by time period after each trading entity has signed the contract; d_{sp}, d_{ti} are the spatial and temporal dimensions of electricity resources in the spot market, respectively. Therefore, the product extension model of compensation price in the database is obtained as:

$$f_{CP} = \theta_{su} \left(M_v, Q_{PGC} \right) M_b \tag{3}$$

where f_{CP} is the extended product function of the compensation price; $\theta_{su}(\cdot)$ is the difference function; M_b is the attribute of the electricity price metric in the multidimensional cubic database; and on the basis of the cyclic computation of the spatial and temporal dimensions of the multisubjects in the database to get the result of its compensation calculation is:

$$C_{co} = \theta_f \left(f_{CP}, \{ d_{sp}, d_{to} \} \right) \tag{4}$$

where C_{co} is the compensation price settlement result of the spot market in the previous day; θ_f is the iterative operation function in the multidimensional cubic database.

Because of the maintenance of the entire power system operation by the operator in the power market spot transaction is taken into account, the compensation gain generated by the operator will be added to the clearing optimization model as an additional price.

2.2 Based on the source network, load and storage joint system planning model

2.2.1 Outer planning model

The outer planning model contains 2 objectives, which are as follows.

1) Maximize the PV local consumption rate:

$$\max R_{PV} = \frac{\sum_{t=1}^{N_t}\sum_{s=1}^{N_s} P_r(s)\cdot\left(P_{pl,s}^t + P_{pc,s}^t\right)}{\sum_{t=1}^{N_t}\sum_{s=1}^{N_s} P_r(s)\cdot P_{PV,s}^t} \tag{5}$$

where: R_{PV} is the PV in-situ consumption rate; N_t is the total time; and N_s is the number of reduced scenarios; $P_r(s)$ is the probability of occurrence of each scenario; $P_{PV,s}^t$ is the total distributed PV power generation under scenario s at moment t after cutting down the distributed PV active output; $P_{pl,s}^t$ is the distributed PV power consumed by the load under scenario s at moment t after curtailment of distributed PV active output; $P_{pc,s}^t$ is the distributed PV power consumed by the savings battery under the t moment scenario s after cutting down the distributed PV active output.

2) Maximize the investment return of the combined photovoltaic storage system.

The life cycle investment return λ maximization objective is:

$$\max \lambda = B_p - C_p \tag{6}$$

where: B_p is the annual life cycle benefit; C_p is the annual life cycle investment cost:

$$B_p = \sum_{t=1}^{N_t}\sum_{s=1}^{N_s} P_r(s)\cdot p_{P2g}\cdot I_{t,s} + \sum_{t=1}^{N_t}\sum_{s=1}^{N_s} P_r(s)\cdot p_b\cdot E_{t,s} \tag{7}$$

where: p_{P2g} is the PV feed-in tariff; $I_{t,s}$ is the total PV feed-in electricity at the t moment; p_b is the government subsidized tariff; and $E_{t,s}$ is the total electricity generation after PV active output abatement at the t moment:

$$C_p = C_{PV} + C_c + C_{g2p} + C_{ILR} \tag{8}$$

where C_{PV} is the distributed PV installation and maintenance cost, i.e:

$$C_{PV} = \frac{r\cdot(1+r)^n}{r\cdot(1+r)^n - 1}\cdot c_{p,m}\cdot E_{PV} \tag{9}$$

where: r is the discount rate; n is the economic service life of distributed PV; $c_{p,m}$ is the installation and operation and maintenance cost of distributed PV per unit capacity; and E_{PV} is the rated total installed capacity.

C_c is the savings battery installation and maintenance cost, i.e:

$$C_c = \frac{r\cdot(1+r)^{n_0}}{r\cdot(1+r)^{n_0} - 1}\cdot c_c\cdot E_c \tag{10}$$

where: n_0 is the economic service life of the battery; c_c is the unit battery installation and operation and maintenance cost; E_c is the total installed capacity of the battery.

C_{g2p} is the cost of purchasing electricity from the main grid, i.e.:

$$C_{g2p} = \sum_{t=1}^{N_t} \sum_{s=1}^{N_s} P_r(s) \cdot p(t) \cdot P_{s,t}^b \tag{11}$$

where: $p(t)$ is the price of electricity purchased from the main grid at moment t; $P_{s,t}^b$ is the amount of electricity purchased from the main grid at moment t under scenario s.

C_{ILR} is the interruption compensation cost, i.e.:

$$C_{ILR} = \sum_{t=1}^{N_t} \sum_{s=1}^{N_s} P_r(s) \cdot p_{dr} \cdot P_{t,s}^{ILR} \tag{12}$$

where: p_{dr} is the compensation cost per unit of interrupted power; $P_{t,s}^{ILR}$ is the total interruptible load interruption at moment t scene s.

2.2.2 Inner layer planning model

The inner layer determines the specific operation plan of the combined optical storage system for each time period according to the following principles, and the inner layer planning takes the minimum average value of the voltage deviation of each node within 24h of each scenario as the optimization objective, and the expression is:

$$\min \Delta f_u = \frac{1}{24} \sum_{t=1}^{24} \left(\frac{1}{N_g} \sum_{g=1}^{N_g} \left| \frac{U_{g,s}^t - U_{OLTC}^s}{U_{OLTC}^s} \right| \right) \tag{13}$$

where: $U_{g,s}^t$ is the voltage magnitude of the g th node of scenario s at moment t after active management measures; U_{OLTC}^s is the voltage magnitude of the first node of the secondary side of the scenario s system after regulating OLTC; N_g is the number of nodes.

2.2.3 Constraints

1) Currents constraints:

$$\begin{cases} P_{i,s} = U_{i,s} \cdot \sum_{j=1}^{N} U_{j,s} \cdot \left(G_{ij} \cos \delta_{ij} + B_{ij} \sin \delta_{ij} \right) \\ Q_{i,s} = U_{i,s} \cdot \sum_{j=1}^{N} U_{j,s} \left(G_{ij} \cos \delta_{ij} - B_{ij} \sin \delta_{ij} \right) \end{cases} \tag{14}$$

where: $U_{i,s}$ and $U_{j,s}$ are the voltages of nodes i and j under scenario s, respectively; $P_{i,s}$ and $Q_{i,s}$ are the active and reactive power injected by node i at scenario s, respectively; G_{ij} and B_{ij} are the conductance and conductance of the system; δ_{ij} is the node voltage phase angle difference.

2) Nodal voltage constraints:

$$U_{i,\min} \le U_i \le U_{i,\max} \tag{15}$$

where: U_i is the voltage of node i after taking active management measures; $U_{i,\max}$ and $U_{i,\min}$ are the upper and lower limits of the node voltage amplitude, respectively.

In this paper, the voltage constraint is realized by imposing the node voltage overrun penalty term P_u, where μ is the penalty factor:

$$P_u = \mu\left[\max\left(U_{i,\min} - U_i, 0\right) + \max\left(U_i - U_{i,\max}, 0\right)\right] \tag{16}$$

3) OLTC secondary side voltage constraints:

$$U_{OLTC}^{\min} \le U_{OLTC} \le U_{OLTC}^{\max} \tag{17}$$

where: U_{OLTC} is the voltage value of the secondary side of the on-load transformer; $U_{OLTC}^{\min}$, $U_{OLTC}^{\max}$ are the upper and lower limits of the voltage value of the secondary side of the on-load transformer.

4) Distributed PV active output reduction rate constraints:

$$0 \le R_{PV,k,s} \le R_{PV,k,s}^{\max} \tag{18}$$

where $R_{PV,k,s}$ and $R_{PV,k,s}^{\max}$ are the s th scenario k th PV active output abatement rate and the maximum allowable abatement rate, respectively.

5) ILR interruption rate constraint:

$$0 \le R_{ILR,m,s} \le R_{ILR,m,s}^{\max} \tag{19}$$

where $R_{\mathrm{ILR},m,s}$ and $R_{ILR,m,s}^{\max}$ are the interruption rate and the maximum allowable interruption rate for the m th ILR of the s scenario, respectively.

6) Saving battery charge state SOC constraint:

$$S_{OC\min} \le S_{OC,t,k} \le S_{OC\max} \tag{20}$$

where: $S_{\mathrm{OC},t,k}$ is the charging state of the capacity of the k th savings battery at the t th moment, and $S_{OC\max}$ and $S_{OC\min}$ are the maximal and minimal charging state of the battery, respectively.

2.3 Improved multi-objective particle swarm algorithm solution model

MOPSO is an optimization approach that controls the movement of particles in a multidimensional search space. It may be applied to multi-objective problems and also used to solve constrained single-objective problems by converting it to a multi-objective problem. The control parameters in particle swarm optimization are *w* and *c*, and the inertia weight is the

parameter that regulates the trade-off between global exploration and local exploitation. The inertia weight and learning coefficients in the conventional MOPSO framework are typically determined at initialization or through a linearly decreasing weighting scheme. The IMOPSO algorithm used in the present work improves this parameter adjustment procedure so that the method could continue to demonstrate high search performance and better optimization performance.

The size of w is dynamically adjusted according to the particle fitness value and the population fitness value:

$$w=\begin{cases} w_{\min}-\left(w_{\max}-w_{\min}\right)\dfrac{f-f_{\min}}{f_h-f_{\min}}, & f_{k,d}<\overline{f}_h \\ w_{\max}, & f_{k,d}\geq\overline{f}_h \end{cases} \tag{21}$$

where $w_{\max}$ and $w_{\min}$ are the upper and lower limits of the inertia weights, f is the value of population fitness, $\overline{f}_h$ is the value of population average fitness, $f_{k,d}$ is the fitness value of the particle d, and h is the number of targets. Through the selection, ensure that the particle can guarantee the forward direction under the premise of faster approach to the Pareto front.

The adjustment of the learning factor can help particles put more weight on positional information about the swarm, which is useful to maintain convergence efficiency and search efficiency; both these effects regulate the fitness of the population.

$$\begin{cases} c_1=c_{\max}-\left(c_{\max}-c_{\min}\right)\dfrac{k}{k_{\max}} \\ c_2=c_{\min}+\left(c_{\max}-c_{\min}\right)\dfrac{k}{k_{\max}} \end{cases} \tag{22}$$

The larger c_1 is the large value of particle search bias, and the larger c_2 is the global optimum of its particle convergence. $c_{\max}$ and $c_{\min}$ are the upper and lower limits of the learning factor, which take the values of 2 and 0.2, respectively.

In the MOPSO algorithm, the particles will move forward with the history and the global optimal particles, which leads to too much aggregation of the particle swarm and falls into the problem of local optimization. To solve this problem, the IMOPSO algorithm adaptively disperses the more concentrated particle swarms during the particle iteration process, realizing the diversity of the population and avoiding the local optimum to achieve the optimal solution of the Pareto frontier. The conditions for its dispersion are:

$$\frac{L_{d,best}}{L_{d,best}}<\varphi_0\left(1-\frac{k}{k_{\max}}\right) \tag{23}$$

where $L_{d,e}$ is the Euclidean distance between particles d and e in s-dimensional space with the value of the objective function as the coordinate; $L_{d,best}$ is the Euclidean distance between particles d and the optimal particles of the population in s-dimensional space; and φ_0 is the initial threshold value. In the early stage of particle optimization, the position of the particle is prioritized to control the position of the particle, enhance the diversity of particles

and global optimization ability, and in the late stage of particle optimization when the particle is close to the global optimal point, the effect of local optimization is improved to enhance the convergence of the whole algorithm, which is given in the following formula:

$$L_d(k) = \frac{k}{k_{\max}} L_d(k) + D\left(1 - \frac{k}{k_{\max}}\right) L_d(k) \tag{24}$$

where $L_d(k)$ is the position of the particle after d iterations k times, D is the position separation factor, the larger the distance between the particles, the larger the separation factor, and its specific formula is:

$$D = \begin{cases} L_{d,e} \times r(-0.5, 0.5) & L_{d,gbest} \geq \ell^{\frac{k}{k_{\max}}} \\ L_{d,e} \times [1 + r(-0.5, 0.5)] & L_{d,gbest} < \ell^{\frac{k}{k_{\max}}} \end{cases} \tag{25}$$

where $r(-0.5, 0.5)$ is the random number distributed on the interval $[-0.5, 0.5]$, $L_{d,gbest}$ is the globally optimal solution of the particle d, and $\ell^{\frac{k}{k_{\max}}}$ is the adaptive threshold.

IMOPSO algorithm is an improvement of convergence behavior and minimizes the chances of being stuck in local optima through adaptive changes of the position division factor, which allows particles to search more effectively in optimization.

In order to evaluate the performance of the algorithms, this paper also presents the concept of the global optimization success rate S_{gb}, whose expression is shown below:

$$S_{gb} = \frac{G_s}{G_{all}} \times 100\% \tag{26}$$

where G_{all} denotes the total number of experiments; G_s denotes the number of experiments that find the optimal solution among all experiments.

The flow of IMOPSO algorithm to solve the integrated cooperative planning model of source network, load and storage is shown in Fig. 2.

Step1: Initialize the particle population, randomly generate the position and velocity of each particle, set the size of the population, and divide the population.

Step2: Determine the objective function, $f_1 \sim f_n$.

Step3: Calculate the value of the objective function and the value of the fitness of the population:

$$\begin{cases} f_1'(x) = \dfrac{1}{1 + c + f_1(x)} \\ \cdots\cdots \\ f_n'(x) = \dfrac{1}{1 + c + f_n(x)} \\ c \geq 0,\ c + f(x) \geq 0 \end{cases} \tag{27}$$

where $f_1'(x)$ and $f_n'(x)$ are the fitness of the objective function under the computational subgoal, c is the objective function bounds estimate, and $f(x)$ is the fitness of the globally optimal objective function, respectively.

Step4: Merge the parent and child populations to calculate the crowding degree.

Step5: Determine if the set iteration limit has been achieved. If the condition is not satisfied, reinitialize particle velocities and positions and implement adaptive particle partitioning based on the dispersion behavior of the swarm.

Step6: Calculate the particle Pareto optimal solution, update the historical optimal and global optimal.

Step7: When iteration limit has been reached, end the process and print the end global optimal solution set with the respective objective-function values.

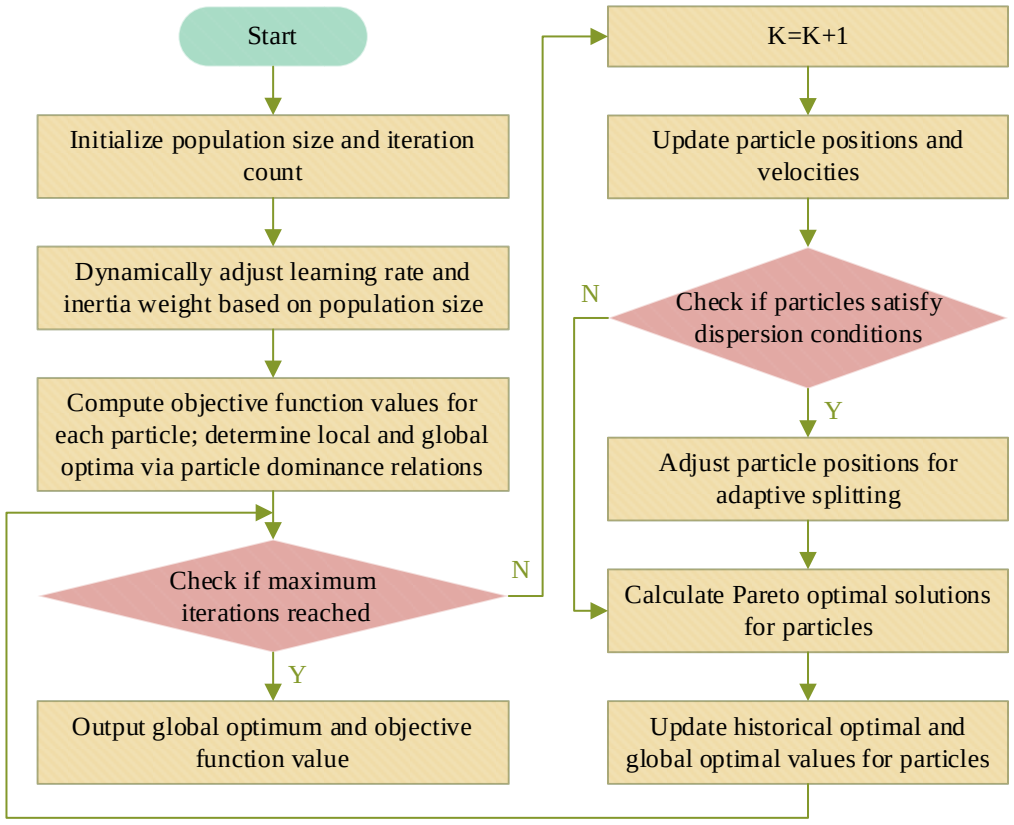

Figure 2: The Solution Process of IMOPSO Algorithm for Source-grid-load-storage

3 Performance of IMOPSO algorithm and its arithmetic simulation in source network load storage

This paper uses the standard benchmark functions ZDT1, ZDT2, and ZDT3 to assess the performance of IMOPSO within the source-grid-load-storage coordination framework, and explores the optimization outcomes and numerical simulation of active distribution network operation with the integrated planning strategy proposed. The effectiveness of the optimization framework is then analyzed using the following three scenarios depending on the installed capacities of thermal power, hydropower, wind power, photovoltaic generation, and energy storage.

Scenario 1: Only the source-grid-load coordinated operation scheme is considered and the multi-energy complementary generation planning framework is not considered.

Scenario 2: Based on the optimized dispatching scheme of case 1, the power output schedule is given to the sending-end generation resources and the multi-energy complementary generation planning framework has not been implemented.

Scenario 3: Also, yet another power-supply planning element is included, and the integrated configuration framework developed in this paper is used to plan and operate the multi-energy complementary system subject to source-grid-load coordination.

3.1 Performance analysis of the IMOPSO algorithm

3.1.1 IMOPSO algorithm performance metrics

(1) Diversity metric η

If the Pareto-optimal front developed by the chosen algorithm is the same with the real Pareto front, $d_f = d_l = 0$, all $d_i = \bar{d}$, at this time $\eta = 0$, η the smaller, the better the diversity of the algorithm. That is:

$$\eta = \frac{d_f + d_l + \sum_{i=1}^{n-1} \left| d_i - \bar{d} \right|}{d_f + d_l + (n-1)\bar{d}} \tag{28}$$

where: d_i - the distance between two adjacent points in the non-inferior optimization target region.

$\bar{d}$ - the mean value of d_i.

d_f, d_l - distance between the boundary solution and the extreme solution.

n - number of non-inferior solutions.

(2) Convergence index

In case when the actual Pareto front of the target multi-objective optimization model is available, some representative points may be chosen on this front and the average distance between them and the solution set obtained by the chosen algorithm can be found. The lower the metric, the better convergence performance of the algorithm.

3.1.2 Algorithm testing

The benchmark functions used in this work to measure the performance of IMOPSO are the standard ones, ZDT1, ZDT2 and ZDT3. The test functions are described in detail in Table 1. The key parameters of the IMOPSO are defined in the following way: the upper limit of the inertia weight $\omega_{\max} = 0.9$, the lower limit of the inertia weight $\omega_{\min} = 0.2$, the acceleration constant $c_1 = c_2 = 2$, the radius of the small habitat is 0.5, the population size is 180, and the maximum number of iterations is 150.

Table 1: Specific Description of IMOPSO Test Function

ZDT1	ZDT2	ZDT3
$\min f_1(x) = x_1$	$\min f_1(x) = x_1$	
$\min f_2(x) = g(x)\left(1-\sqrt{f_1(x)/g(x)}\right)$	$\min f_2(x) = g(x)h(f_1(x), g(x))$	$\min f_2(x) = g(x)h(f_1(x), g(x))$
$g(x_2,\cdots,x_{10}) = 1+9\sum_{i=2}^{10} x_i$	$g(x) = 1+\frac{9}{29}\sum_{i=2}^{10} x_i$	$g(x) = 1+\frac{9}{29}\sum_{i=2}^{30} x_i$
$0 \le x_i \le 1; 1 \le i \le 10$	$h(f_1(x), g(x)) = 1-\sqrt{\frac{f_1(x)}{g(x)}}$	$h(f_1(x), g(x)) = 1-\sqrt{\frac{f_1(x)}{g(x)}} - \left(\frac{f_1(x)}{g(x)}\right)\sin(10\pi f_1(x))$
	$0 \le x_i \le 3; 1 \le i \le 10$	$0 \le x_i \le 1; 1 \le i \le 30$

The results of the comparison between the ZDT1 test function and the real solution are shown in Fig. 3. The simulation test results show that the results obtained by the IMOPSO algorithm test function ZDT1 are consistent with the real Pareto frontiers, indicating the correctness of the algorithm.

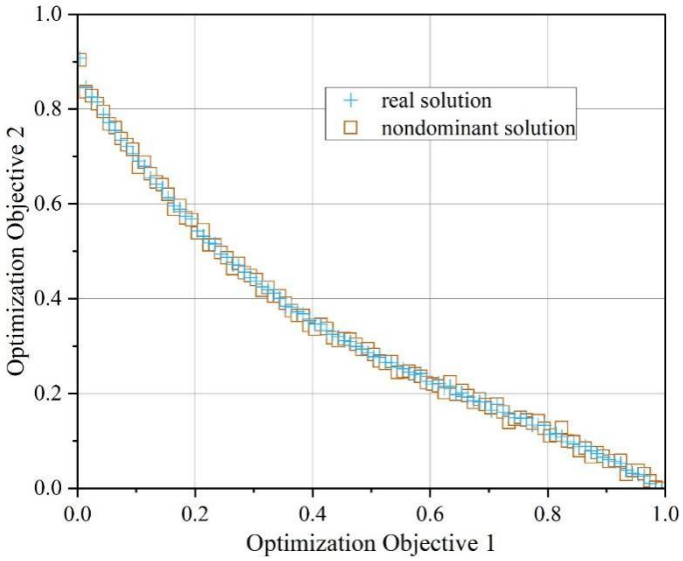

Figure 3: Comparison of ZDT1 test function and real solution

The ZDT2 benchmark function was also optimized under the same experimental settings by means of the IMOPSO algorithm and as shown in Fig. 4, a comparison is made between the achieved results and the actual Pareto front. The simulation evidence shows that the solution space produced to ZDT2 is almost identical to the real Pareto front, as it indicates that IMOPSO is effective in terms of its performance on the models of different dimensions and computational complexity.

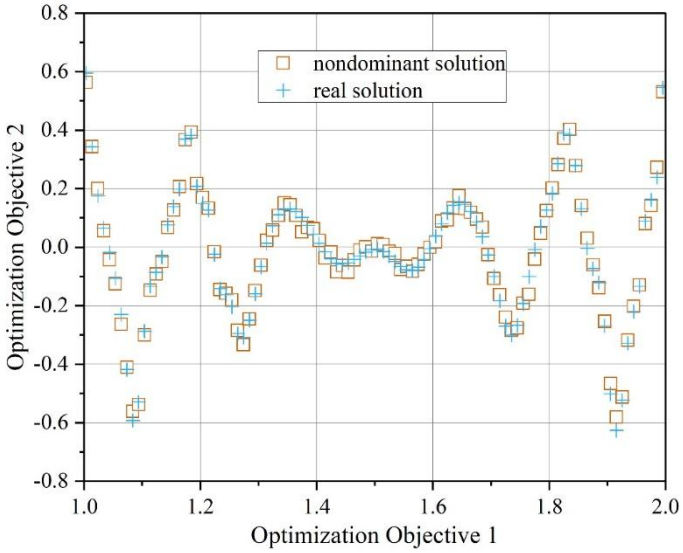

Figure 4: Comparison of ZDT2 test function and real solution

The results of the comparison between the ZDT3 test function and the real solution are shown in Fig. 5. The simulation test results show that the solution results of the IMOPSO algorithm test function ZDT3 are consistent with the real Pareto front, which further indicates that the IMOPSO algorithm has good solution results for models with different dimensions and different computational complexity.

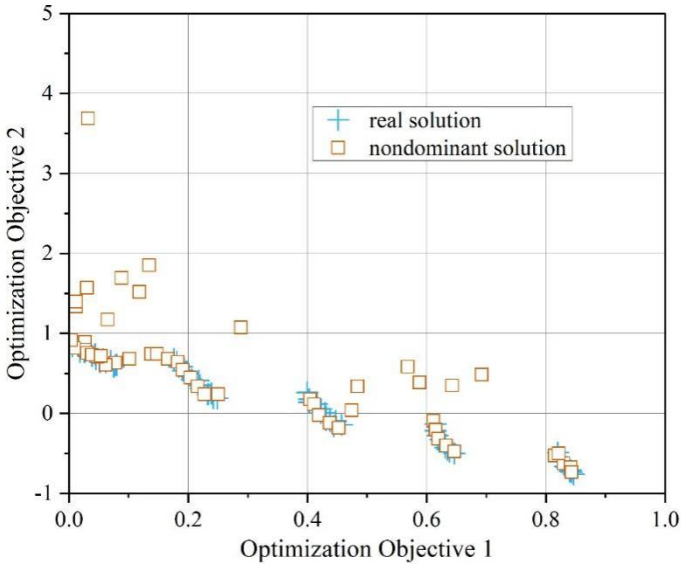

Figure 5: Comparison of ZDT3 test function and real solution

3.1.3 Algorithm performance comparison

In order to illustrate the benefits of the enhanced particle swarm optimization approach presented in this work, the ZDT2 benchmark function has been used to test the performance of the algorithms prior to the modification and post-modification. As shown in Figure 6, the distribution of the frontier solutions found by MOPSO is given, and Figure 7 shows the same distribution produced by IMOPSO. The comparison shows that the enhanced multi-objective particle swarm optimization algorithm can produce more Pareto-front solutions and reach a higher level of agreement with the real front.

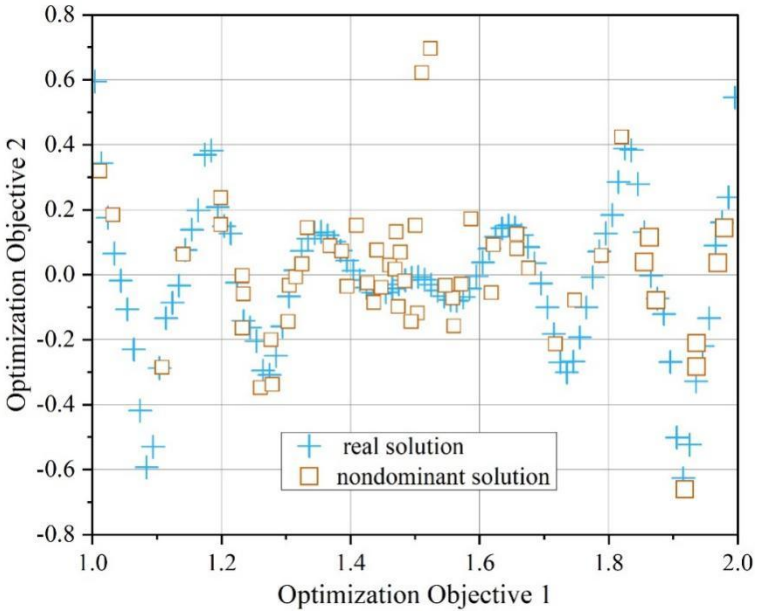

Figure 6: MOPSO front solution distribution

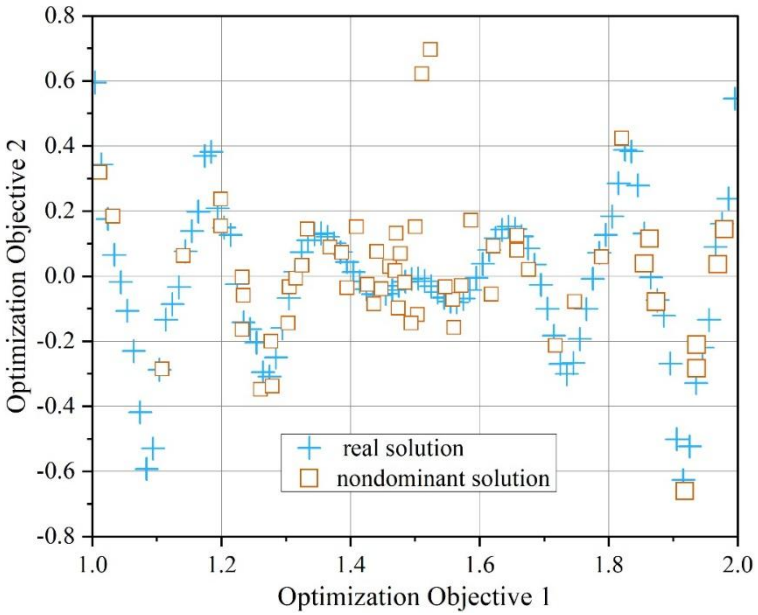

Figure 7: IMOPSO frontier solution distribution

In order to explore how the two approaches behave in more depth, this paper runs both the traditional MOPSO and the IMOPSO models 60 times at the set parameters, and then assesses mean values and variances of the convergence measure, diversity measure and time of execution. Table 2 reports the corresponding comparison findings. The findings suggest that, in every one of the three benchmark functions, the IMOPSO has better performance than the conventional MOPSO method not only in convergence measures, but also in terms of average diversity values, which clearly show superiority in the convergence quality as well as in population distribution. Furthermore, following 20 computational experiments, the duration needed by IMOPSO to deliver a solution is less than the traditional method. As a whole, the suggested IMOPSO approach shows a better behavior compared to the standard MOPSO in both optimization efficacy and computational efficacy.

Table 2: The Correlation Performance of Two Algorithms

Metric	Algorithm	Convergence index	Test1	Test1	ZDT3
Convergence index comparison	MOPSO	Mean	0.0238	0.0229	0.0068
		Variance	3.57×10^{-6}	1.62×10^{-5}	3.28×10^{-7}
	IMOPSO	Mean	0.0071	0.0072	0.023
		Variance	1.33×10^{-7}	1.72×10^{-7}	4.02×10^{-7}
Diversity index comparison	MOPSO	Mean	0.3394	0.4895	0.5603
		Variance	0.0015	0.0031	0.0049
	IMOPSO	Mean	0.3603	0.2501	0.5536
		Variance	0.0014	0.0004	0.0002
Average runtime(s)	MOPSO	Mean	161.03	174.13	165.14
	IMOPSO	Mean	149.96	162.16	150.36

3.2 Optimized Model Arithmetic Simulation

3.2.1 Parameterization of the algorithm

This subsection is where the simulation and verification of the integrated planning-operation framework of a multi-energy complementary system during the source-grid-load coordination is carried out. The installed capacity limits of thermal power, hydropower, wind power, photovoltaic generation, and energy storage are established as 10,000 MW, 20,000 MW, 10,000 MW, 12,000 MW and 10,000 MW respectively. The main parameters of the generating units are presented in Table 3.

Table 3: Generator set equipment parameters

Power generation technology	Unit capacity investment cost/(¥·kW^{-1})	Unit capacity O&M cost/(¥·kW^{-1})	Equipment service life/a
Thermal power generation	3542.23	64.49	42
Hydroelectricity	11361.54	100.95	85
Wind electricity	7721.36	223.6	26
Photovoltaic	7263.31	71.88	26
Stored energy	15365.23	69.92	18

3.2.2 Analysis of the Generation Results of Typical Operational Scenarios

In order to fully retain the temporal characteristics of wind power and load demand characteristics, this paper, according to the idea of typical scenario generation, selects the 360*24h wind power data and local load demand characteristics, as well as the UHV DC transmission power as the original operating scenarios, and adopts PFS-based K-means clustering algorithm to reduce the original operating scenarios, and extracts a representative "wind-optical-load" typical operating scenarios. The K-means clustering algorithm based on PFS is used to reduce the original operation scenarios and extract the typical operation scenarios with a certain degree of representativeness. Since the number of original scenes in this paper is 360, the effective search range of the number of clusters k is $\left[2,\sqrt{360}\right]$. It is found that when the number of clusters is 4, the value of PFS is the largest. Therefore, the clustering result corresponding to k=4 is the typical scene running curve sought in this paper. The typical scenario operation curves are shown in Fig. 8, where (a) ~ (d) represent four typical scenarios of wind power, photovoltaic, local load and outgoing power, respectively.

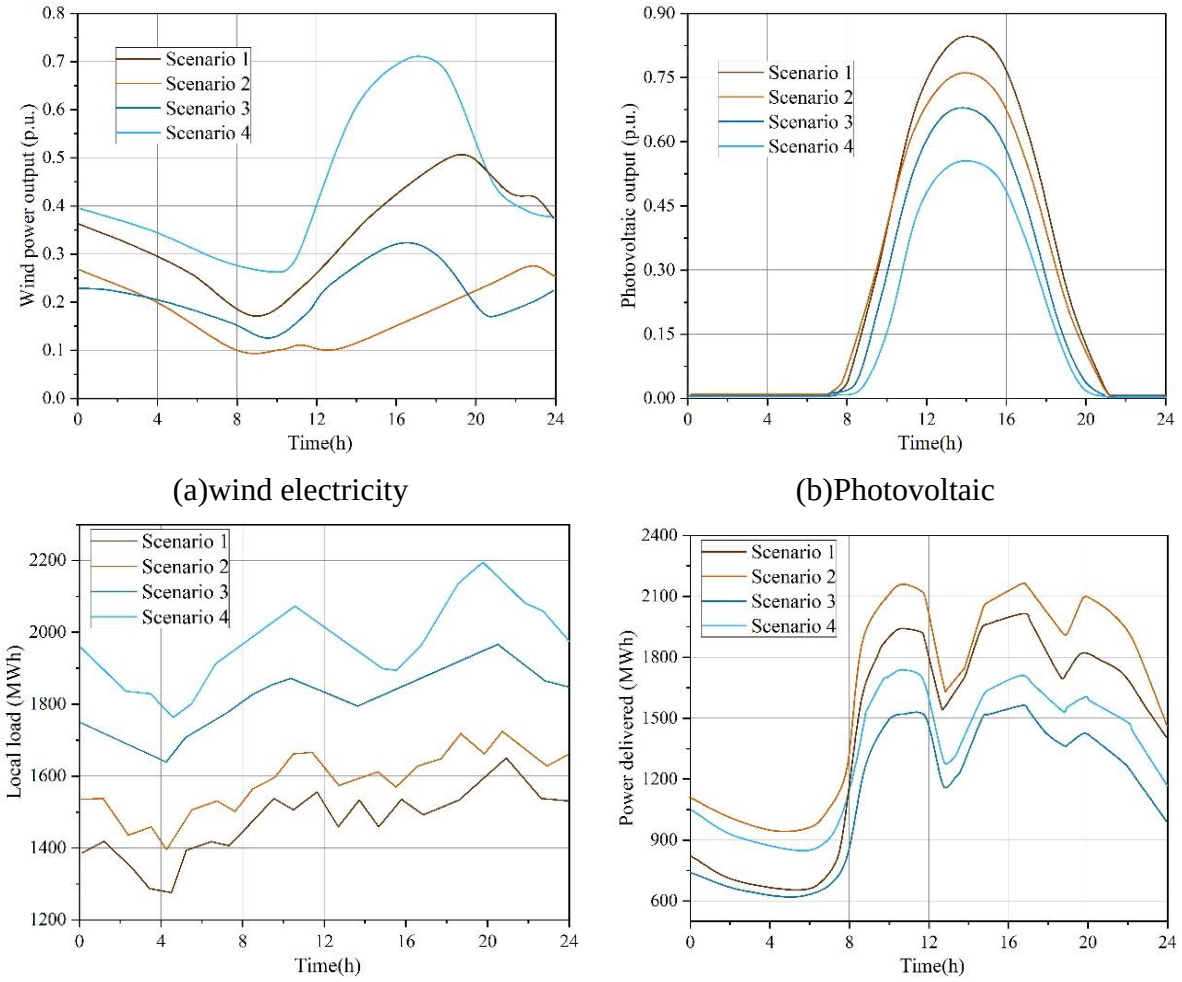

(a)wind electricity (b)Photovoltaic

(c)Local load (d)Output power

Figure 8: Typical scenario operation curve

The scene probabilities of the four typical scenarios are also obtained as shown in Table 4. It can be found that all three types of curves are able to summarize their respective output characteristics in a more comprehensive way, and have good representativeness, which can be used as typical scenarios in the content of the subsequent study.

Table 4: Scenes probability of 4 typical scenarios

Typical Scenario	Original scene sample count	Number of typical scenario samples	Scenario probability (%)
Typical Scenario 1	360	128	35.56
Typical Scenario 2	360	67	18.61
Typical Scenario 3	360	125	34.72
Typical Scenario 4	360	40	11.11

3.2.3 Analysis of the results of the planning and operational integration configuration

By applying the integrated configuration framework suggested in this paper to the planning and operation of a multi-energy complementary system with source-network-load coordination, the enhanced multi-objective particle swarm method has been applied in MATLAB to solve the

planning layer and the operational layer sequentially. It will give you the best installation size of generation units and their corresponding dispatch plan to operate the system at the same time. Table 5 displays the results of the optimized capacity-allocation in the generation portfolio. The capacities of thermal power, hydropower, wind power, and photovoltaic units, as well as energy storage, installed are 1110 MW, 2465 MW, 4100 MW, 3000 MW, and 995 MW respectively. Out of these five technologies, wind power has the biggest share and then photovoltaic units. Furthermore, photovoltaic generation is less expensive when compared to the other two clean-energy choices, i.e., wind and hydropower. Nevertheless, the fact that outputs of wind and solar cannot be predicted or controlled leads to the need to cut down power generation when there is an overproduction of renewable energy, whereas the lack of sufficient wind, solar, and hydropower can occur in dry seasons. This is why a particular level of energy storage should be utilized to transfer electricity across the time interval, and thermal generators are also needed to fill the remaining gap in supply.

Table 5: Result of Optimal Installation Configuration of Power Generation Equipment

Power generation technology	Thermal power generation	Hydroelectricity	Wind electricity	Photovoltaic	Stored energy
Installed capacity MW	1110MW	2465MW	4100MW	3000MW	995MW

In order to minimize the wind and light discard rate of the multi-energy complementary power generation system during operation, the operation level adopts the principle of wind and water clean energy priority generation on the basis of the source-network-load synergistic optimization operation model constructed in this paper. Figure 9 shows the operation scheduling scheme of power generation equipment under typical scenarios, where (a) ~ (d) represent the unit output results of scenarios 1 ~ 4, respectively. From the figure, it can be seen that since the PV unit output is 0 in the early morning and evening, the output power of the power generation system is prioritized to come from the WTGs, and the part of the insufficient load demand is then supplemented by the hydroelectric units, energy storage equipment and thermal power units. When the wind speed and light intensity during the day is small, the wind and light output power supply is insufficient to give priority to the hydropower unit to supplement the part of the hydroelectric unit, hydroelectric unit discharge power is not satisfied when the maximum power is not met by the energy storage equipment discharge, thermal power unit power generation, exceeding the maximum output limit of the part of the load-cutting operation is considered.

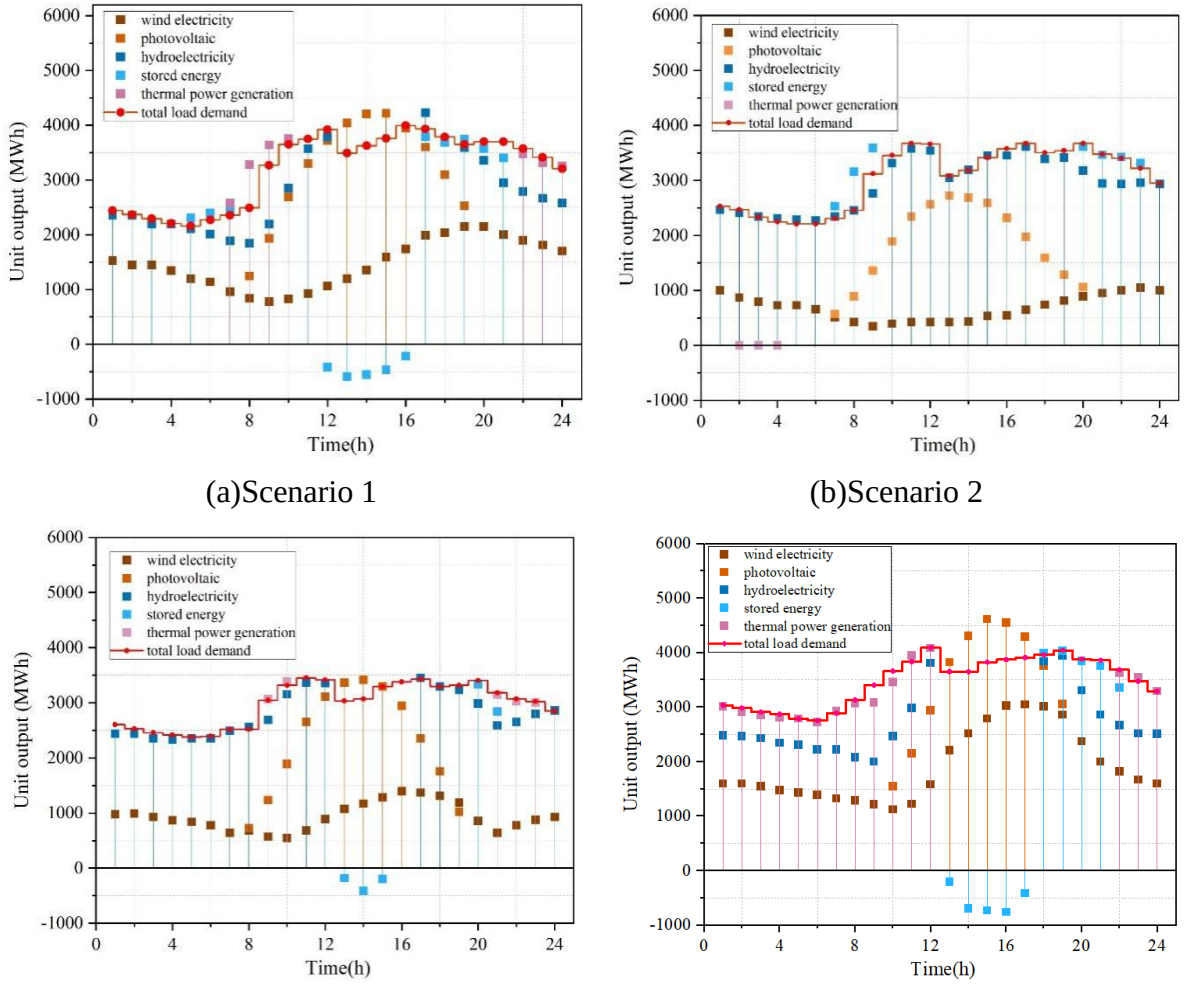

Figure 9: Scheduling scheme of power generation equipment operation

3.2.4 Validation of model validity

The comparative analysis of the feasibility and effectiveness of the sending-end grid output schedule established at the operational stage, as well as the integration of the planning-operation configuration framework of the multi-energy complementary system in the context of source-network-load coordination suggested in this paper is discussed in this subsection. The optimization outcomes of all three cases are shown in Table 6.

Through comparison between Case 1 and Case 2 we can obtain that wind and solar curtailment cost in Case 2 is 0.00. This result means that there is no curtailment of renewables in the optimal dispatch of Case 2, since renewable generation is less than the total responsive load demand, and the rest of the deficit is met by storage discharge and thermal generation. Case 3 also includes power supply planning module based on Case 2. Despite the fact that load shedding cost and fuel cost in Case 3 are greater than in Case 2, the overall economic cost is much lower, implying that the integrated planning operation structure is more efficient in enhancing the economic efficiency of the multi energy complementary generation system.

Table 6: Three schemes planning optimization results

scheme	Solution 1	Solution 2	Solution 3
thermal power generation /MW	1384	1391	1112
hydroelectricity /MW	2497	2498	2458
wind electricity /MW	4610	4614	4184
photovoltaic /MW	2901	2902	3100
stored energy /MW	1482	1504	996
Total economic cost / billion yuan	114.9	124.22	103.39
Total operating cost per 10,000 yuan	525.43	304.27	917.37
Cost of wind and solar curtailment (RMB 10,000)	221.01	0.00	0.00
load cost per 10,000 yuan	0.00	0.00	574.65
Fuel consumption cost per 10,000 yuan	314.58	297.47	380.73
Carbon emissions per ton	3987.39	3754.87	4723.85

4 Conclusion

The article deeply analyzes the spot market trading mechanism of the revenue allocation of source network and load storage, based on which the outer layer planning model and inner layer planning model of the joint system of source network and load storage are constructed, and multiple sets of constraint functions are designed to limit the feasible range of the optimal solution. The optimal solution search adopts the IMOPSO algorithm, which is dynamically adjusted by the learning factor to ensure the best convergence speed and search effect. The performance and effectiveness of the algorithm are simulated and tested, and the following results are obtained:

The solution results of IMOPSO algorithm under three different test functions “ZDT1, ZDT2 and ZDT3” are consistent with the real Pareto front, which shows that IMOPSO algorithm has a good solution effect for models with different dimensions and computational complexity.

The output strategy of source-grid-load-storage integrated model developed in this work is based entirely on the principle of clean energy dispatch, which reduces the fuel use and carbon-emission expenses of thermal power, maximizes the use of renewable energy, reduces the peak-regulation stress on both ends of the grid and improves the general economic efficiency of the multi-energy complementary generation system.

References

[1] Yu, X., Wang, B., Wang, W., Guo, X., Han, J., & Chen, X. (2022). Analysis of renewable resources in Central China under the “double carbon” strategy. Energy Reports, 8, 361-373.

[2] Martinot, E. (2016). Grid integration of renewable energy: flexibility, innovation, and experience. Annual Review of Environment and Resources, 41(1), 223-251.

[3] McPherson, M., & Tahseen, S. (2018). Deploying storage assets to facilitate variable renewable energy integration: The impacts of grid flexibility, renewable penetration, and market structure. Energy, 145, 856-870.

[4] Purkait, P., Basu, M., & Nath, S. R. (2024). Renewable energy integration to electric

power grid: opportunities, challenges, and solutions. Challenges and opportunities of distributed renewable power, 37-100.

[5] Zhu, B., Zheng, X., Shen, S., Jiang, Y., Zhang, Z., Huang, Y., ... & Lin, Z. (2020, October). Development path of future power grid with high proportion of renewable energy in the context of electricity spot market. In 2020 IEEE 4th Conference on Energy Internet and Energy System Integration (EI2) (pp. 3827-3831). IEEE.

[6] Peng, X., & Tao, X. (2018). Cooperative game of electricity retailers in China's spot electricity market. Energy, 145, 152-170.

[7] Zang, T., Wang, S., Wang, Z., Li, C., Liu, Y., Xiao, Y., & Zhou, B. (2024). Integrated planning and operation dispatching of source–grid–load–storage in a new power system: A coupled socio–cyber–physical perspective. Energies, 17(12), 3013.

[8] Li, Y., Zhang, S., Yang, L., Gong, Q., Li, X., & Fan, B. (2024). Optimal scheduling strategies for electrochemical energy storage power stations in the electricity spot market. Frontiers in Energy Research, 12, 1469594.

[9] Ni, Q., Zhang, C., Meng, Z., Huang, Y., Jiang, Y., Sun, W., ... & Lin, Z. (2020, November). Power system economic planning considering "source-grid-load-storage" coordination operation. In 2020 International Conference on Smart Grids and Energy Systems (SGES) (pp. 1000-1004). IEEE.

[10] Shi, Y., Zhang, L., Yang, Y., Li, Q., & Zhang, H. (2025). A review on the short-term strategy for reducing the peak-valley difference and the long-term energy structure optimization strategy in cities based on the integration of "power generation-power grid-power load-Energy storage". Frontiers in Energy Research, 13, 1538811.

[11] Shang, W., Liu, Y., Zhao, L., Pan, S., & Pan, F. (2025). Research on Power Demand Response and Operation Optimization Model in Source-grid-load-storage Integration Project. Strategic Planning for Energy & the Environment, 44(3).

[12] Liu, Y., & Liu, M. (2025, April). Optimization Method of Energy Storage Power Station Capacity Configuration Based on Electricity Spot Joint Market Revenue. In 2025 4th International Conference on New Energy System and Power Engineering (NESP) (pp. 425-430). IEEE.

[13] Wang, X., Gao, X., Ji, Z., Sun, W., Yan, B., & Sun, B. (2025). Dual-layer scheduling coordination algorithm for power supply guarantee using multi-objective optimization in spot market environment. Energy Informatics, 8(1), 37.

[14] Panda, S., Mohanty, S., Rout, P. K., Sahu, B. K., Parida, S. M., Kotb, H., ... & Shouran, M. (2022). An insight into the integration of distributed energy resources and energy storage systems with smart distribution networks using demand-side management. Applied Sciences, 12(17), 8914.

[15] Babatunde, O. M., Munda, J. L., & Hamam, Y. (2019). A comprehensive state-of-the-art survey on power generation expansion planning with intermittent renewable energy source and energy storage. International Journal of Energy Research, 43(12), 6078-6107.

[16] Lu, T., Zhang, W., & Ding, X. (2021). Operation strategy of electricity retailers based on energy storage system to improve comprehensive profitability in China's electricity spot market. Energies, 14(19), 6424.

[17] Hong, F., Liang, B., Ji, W., Jia, X., Wei, B., & Hao, J. (2025). A coordinated optimization strategy of hybrid energy storage capacity configuration and wind power integration in the spot market. Journal of Energy Storage, 131, 117423.